LUND UNIVERSITY

Time-gated viewing studies on tissue -like phantoms

Berg, R; Andersson-Engels, Stefan; Jarlman, O; Svanberg, Sune

Published in:
PROCEEDINGS OF OPTICAL BIOPSY

DOI:
10.1117/12.166819

1994

Link to publication

Citation for published version (APA):
Berg, R., Andersson-Engels, S., Jarlman, O., & Svanberg, S. (1994). Time-gated viewing studies on tissue -like phantoms. In R. Cubeddu, S. Svanberg, H. VandenBergh, & A. Katzir (Eds.), *PROCEEDINGS OF OPTICAL BIOPSY* (Vol. 2081, pp. 137-146). SPIE. https://doi.org/10.1117/12.166819

Total number of authors:
4

General rights
Unless other specific re-use rights are stated the following general rights apply:
Copyright and moral rights for the publications made accessible in the public portal are retained by the authors and/or other copyright owners and it is a condition of accessing publications that users recognise and abide by the legal requirements associated with these rights.
• Users may download and print one copy of any publication from the public portal for the purpose of private study or research.
• You may not further distribute the material or use it for any profit-making activity or commercial gain
• You may freely distribute the URL identifying the publication in the public portal

Read more about Creative commons licenses: https://creativecommons.org/licenses/

Take down policy
If you believe that this document breaches copyright please contact us providing details, and we will remove access to the work immediately and investigate your claim.

LUND UNIVERSITY

PO Box 117
221 00 Lund
+46 46-222 00 00

Download date: 18. Dec. 2025

Invited Paper

Time-Gated Viewing Studies on Tissue-like Phantoms

R. Berg, S. Andersson-Engels, O. Jarlman* and S. Svanberg

Department of Physics, Lund Institute of Technology, P.O. Box 118, S-221 00 Lund, Sweden

***Department of Diagnostic Radiology, Lund University Hospital, S-221 85 Lund, Sweden**

Abstract

A time-gated technique to enhance viewing through highly scattering media, such as tissue, is discussed. Experiments have been performed on tissue-like plastic phantoms in order to determine the possibilities and limitations of the technique. The effects of time-gate width, refractive index, localisation and size of hidden objects have been studied. A computer model to simulate light propagation in tissue is also presented. The model is compared to experimental results.

1. Introduction

The challenge of looking through highly scattering materia, such as tissue, using low-energy photons is a growing field of interest.[1] The task is motivated by a desire to produce a method to do screening for breast cancer using safe doses of optical radiation instead of potentially harmful ionising X-rays.[2,3] The interesting wavelength region is approximately 650-1300 nm where the transmission of tissue is highest.[4] The dilemma when performing breast imaging at these wavelengths is that the dominating attenuation process is scattering. This leads to blurred images and poor resolution. Typical values for the scattering coefficient (μ_s) of tissue are in the range of 10-50 mm^{-1}. This implies that the main part of photons that have travelled through a few centimetre of tissue have been scattered several thousand times.

Several new techniques to improve tissue transillumination imaging are under development.[5,6] The new modalities can be divided into two major groups: time-domain and frequency-domain. The time-domain methods are based on irradiating the tissue with ultra-short laser pulses and perform time-resolved detection of the transmitted light. An enhanced image of objects located deeply inside the tissue can be accomplished, by focusing on the very first arriving photons, which have travelled the straightest and shortest path through the tissue. Different methods of performing time-resolved detection have been used. One technique is based on holographic detection, in which the first transmitted photons are gated out by using the coherent interference between this light and a gate pulse on a holographic plate.[7,8] This technique implies, due to the demand of coherence, that there is an unscattered part of the light exiting from the tissue. This makes this technique in practice not useful for transilluminating some cm of tissue. Other techniques are based on ultra-fast gating by using different types of non-linear optical phenomena[9] like a Kerr shutter[10] or stimulated Raman amplification.[11] These techniques require lasers with very high peak intensities to drive the non-linear optical device. Time-resolved detection can also be attained using fast electronic devices. The streak camera gives a temporal resolution in the order of 1-10 psec, depending on what mode it is operated in, and it has been used by some groups for tissue transillumination studies.[12,13] In this paper we present work performed using time-correlated single photon counting as detection technique.[14] This modality has a temporal resolution of roughly 30-100 psec and the dynamic range is very good.

The frequency-domain approach for tissue transillumination is based on irradiating the sample with intensity modulated light and detecting the change of amplitude and phase of the exiting light.[15,16] As light sources RF-modulated diode lasers and mode-locked lasers have been used. The detection is based on heterodyning or frequency mixing.

The time- and frequency-techniques can also be used for tissue characterisation. By analysing the transmitted or back scattered light the optical properties of the tissue can be determined. These properties are interesting for e.g. photodynamic therapy or tissue diagnostics. The tissue oxygenation can also be determined using these techniques.[17,18]

The conventional transillumination breast imaging (diaphanography) is based on detecting tumors due to the elevated absorption caused by the increased blood supply that many tumors have. However, we have shown that the time-gated technique is much more sensitive to the scattering coefficient than the absorption coefficient.[19] In this paper we show the ability of our system to detect tumour-phantoms depending on their size and localisation in the tissue phantom. We also verify our experimental data using a numerical model developed at our department.[20]

0-8194-1348-8/94/$6.00

Downloaded from SPIE Digital Library on 01 Jul 2011 to 130.235.188.41. Terms of Use: http://spiedl.org/terms

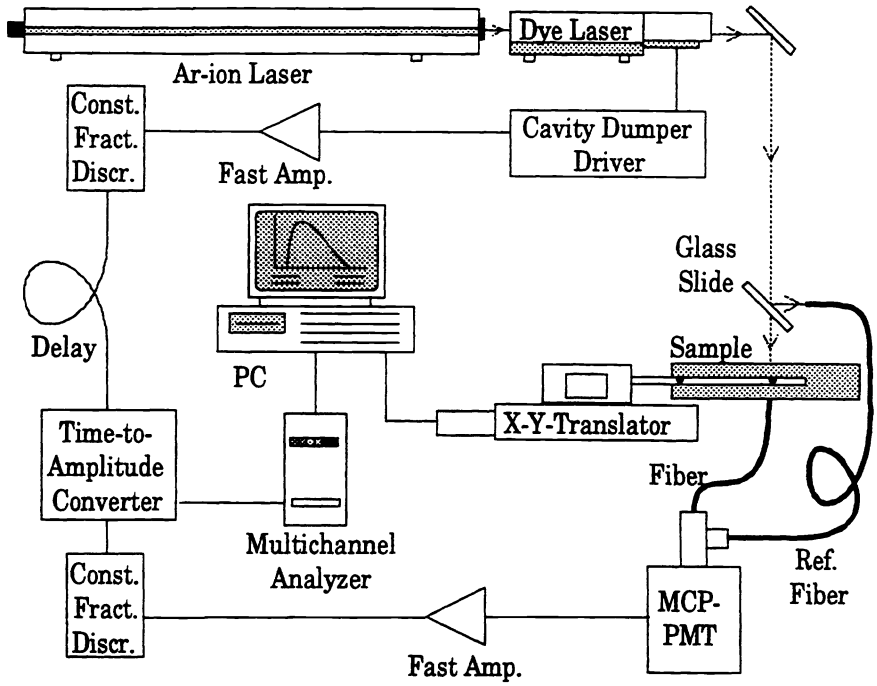

Fig. 1. The experimental set-up used in the time-gated viewing experiments.

2. Materials and Methods

2.1 The experimental set-up

The experimental arrangement used for time-resolved transillumination is illustrated in Fig. 1. The light source was a mode-locked argon-ion laser pumping a dye-laser. The pulse length from the dye-laser was measured with an autocorrelator to be 6 psec. The dye laser was equipped with a cavity dumper, making it possible to alter the repetition rate from the laser. In all the experiments in this paper the repetition rate was 10 MHz and the wavelength 670 nm. The average power was approximately 50 mW. The laser light irradiated the sample and the transmitted light was collected on the opposite side by a 600 μm optical bare fiber. The light exiting the fiber was focused onto the detector through an interference filter to reduce the influence of ambient light. Time-correlated single photon counting detection technique was used. The system consisted of a Hamamatsu R1564U-07 MCP-PMT as a detector. The signal was amplified with a fast amplifier and fed through a constant fraction discriminator (CFD) and worked as a start signal for the time-to-amplitude converter (TAC). The stop signal was taken from the cavity dumper driver unit through an amplifier and a CFD to the TAC. The output voltage from the TAC was fed to a multichannel analyser where the temporal histograms were assembled. The curves were read out to a PC for on-line evaluation. The computer also controlled the two-dimensional scanning over the sample by means of stepping motors. To compensate for any drift phenomena in the system, a small part of the incident light was reflected off by a glass slide and directed to the detector giving a reference peak in time.

2.2 The tissue phantom

The tissue phantom in all the experiments consisted of a white, highly scattering plastic, called Delrin (Du Pont). The optical properties of the plastic were estimated by fitting an experimental time-dispersion curve of light transmitted through a homogenous slab with the solution to the diffusion equation presented by Patterson *et al.*[21] The optical properties were μ_s'=2.3 mm^{-1} and μ_a=0.002 mm^{-1} (μ_s' is the effective scattering coefficient, *i.e.* (1-g)*μ_s), where g is the scattering anisotropy coefficient (the average of the cosine of the scattering angle), and μ_a the absorption coefficient. The plastic is thus a highly scattering medium with low absorption. We used 5 mm thick slabs of the plastic. Holes of different size where drilled into the plastic to act as tumour phantoms. The holes were empty or filled with liquid to simulate different optical properties of the tumour. By screwing the slabs of plastic together different thickness of the model and positions of the tumour could be obtained. Silicon oil was used between the plastic slabs to reduce the effect of any air pockets.

Downloaded from SPIE Digital Library on 01 Jul 2011 to 130.235.188.41. Terms of Use: http://spiedl.org/terms

2.3 The computer model

Two frequently used techniques for modelling of NIR light fluence in tissue is Monte Carlo simulations[22] and to solve the diffusion approximation of the transport equation.[23,24] The Monte Carlo technique is based on tracing a large number of light rays entering the tissue slab at the source. The scattering events within the tissue are determined by a probability function matching the scattering coefficient. At each scattering event a part of the ray, determined by the absorption coefficient, is absorbed. The scattering angle is given by the scattering phase function. A Monte Carlo algorithm can simulate the photon flux very accurately for a wide range of geometries and optical parameters of the tissue slab. Monte Carlo simulations, however, require high computer capacity to obtain statistically good quality data.

The diffusion equation can be derived from the transport equation if the coherent radiance is neglected and the diffuse radiance is assumed to be only linearly dependent of the direction. Using this approximation the transport equation can be simplified to yield the diffusion equation :

$$\frac{n}{c}\frac{\partial\phi(\mathbf{r},t)}{\partial t} - \nabla(D\nabla\phi(\mathbf{r},t)) + \mu_a\phi(\mathbf{r},t) = S(\mathbf{r},t) \qquad (1)$$

where $\phi(\mathbf{r},t)$ is the diffuse photon fluence rate, c is the speed of light in vacuum, n is the refractive index of the tissue, D is the diffusion coefficient ($D=[3(\mu_a+(1-g)\mu_s)]^{-1}$) and $S(\mathbf{r},t)$ is the photon source. In this equation the tissue is characterised of an absorption and a scattering coefficient (μ_a and μ_s, respectively) and the mean cosine of the scattering function (g). This approximation is valid for the photon fluence rate at a distance from the source and some time after an impulse source injection if $\mu_s(1-g)>>\mu_a$. We are interested of the light fluence rate far from the source but as soon as possible after the irradiation pulse. In this situation the diffusion approximation may not be very accurate. However, here we are interested in qualitative rather than quantitative behaviour, and thus this approximation should be acceptable to study the relative sensitivity of the fluence rate to variations in absorption and scattering coefficients inside a turbid medium.

This equation can be solved analytically in certain simple geometries. For our studies, we choose to use a numerical solution of the diffusion approximation. This model allows to freely vary both the scattering and absorption coefficient within the slab and compare weak signals without problem with photon statistics. The diffusion equation was translated to a difference equation for finite steps of the x-,y-,z- and t-variables and a generalised Crank-Nicholson algorithm for three dimensions, called the alternating-direction implicit method (ADI), was employed. This method solves each spatial dimension separately using a third of a time-step for the x-, y-, and z-dimensions, respectively. The resulting equation for the x-dimension is

$$\begin{aligned}\phi^{t+1/3}_{xyz} - \phi^{t}_{xyz} = \frac{c\Delta t}{3n\Delta^2}\Big[\; & D_{x+1/2yz}(\phi^{t+1/3}_{x+1yz} - \phi^{t+1/3}_{xyz}) - \\ & D_{x-1/2yz}(\phi^{t+1/3}_{xyz} - \phi^{t+1/3}_{x-1yz}) + D_{xy+1/2z}(\phi^{t}_{xy+1z} - \phi^{t}_{xyz}) - \\ & D_{xy-1/2z}(\phi^{t}_{xyz} - \phi^{t}_{xy-1z}) + D_{xyz+1/2}(\phi^{t}_{xyz+1} - \phi^{t}_{xyz}) - \\ & D_{xyz-1/2}(\phi^{t}_{xyz} - \phi^{t}_{xyz-1})\;\Big] - \frac{c\Delta t}{6n}\mu_a(\phi^{t}_{xyz} + \phi^{t+1/3}_{xyz})\end{aligned} \qquad (2)$$

where ϕ^{t}_{xyz} is the fluence rate in the matrix element (x,y,z) at time t, Δt is the time step, Δ is the step size in x, y and z, and $D_{x+1/2yz}$ is the average of the diffusion coefficient in the matrix elements (x,y,z) and (x+1,y,z). Similar equations are obtained for the y- and z-dimensions. In order to solve the x-dimension a tridiagonal system of equations has to be solved for every y- and z- coordinate.

Downloaded from SPIE Digital Library on 01 Jul 2011 to 130.235.188.41. Terms of Use: http://spiedl.org/terms

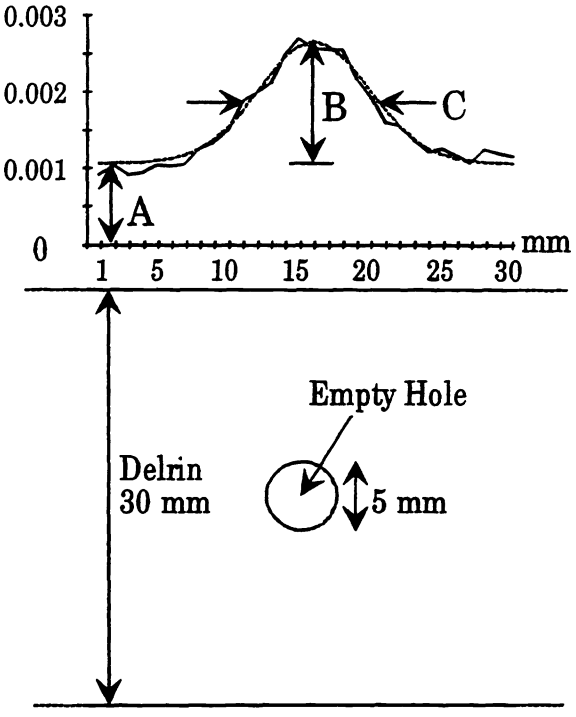

Fig. 2. The geometry used when transilluminating the tissue phantoms. The curve show the relative amount of light detected in the used time-gate window. The different letters (A, B and C) represent the contrast and the width of the hidden object.

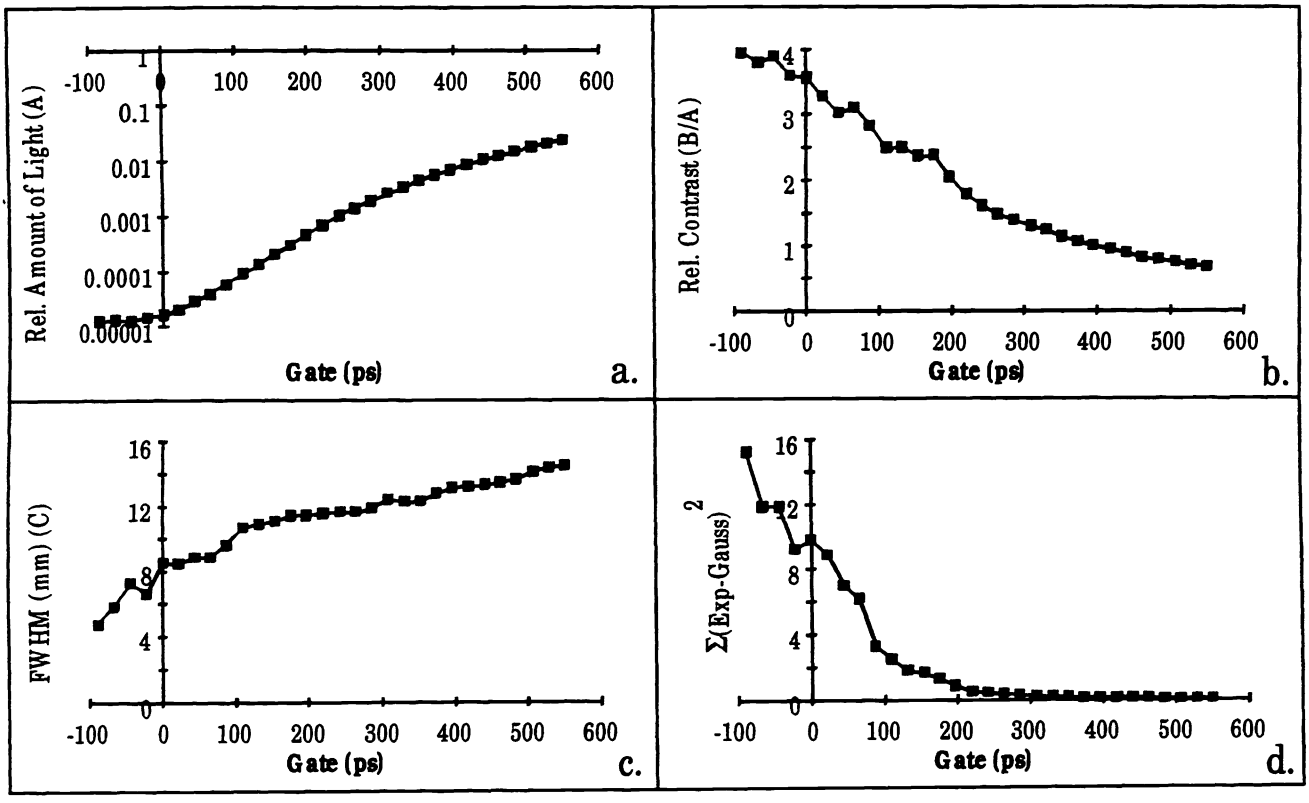

Fig. 3. Influence of the time-gate width when a 30 mm thick tissue phantom containing a 5 mm hole in the middle is transilluminated. a) The relative amount of light detected as a function of the width of the gate window. b) The contrast (B/A). c) The FWHM of the hidden object. d) The residual between the experimental curve and the gaussian fit.

Downloaded from SPIE Digital Library on 01 Jul 2011 to 130.235.188.41. Terms of Use: http://spiedl.org/terms

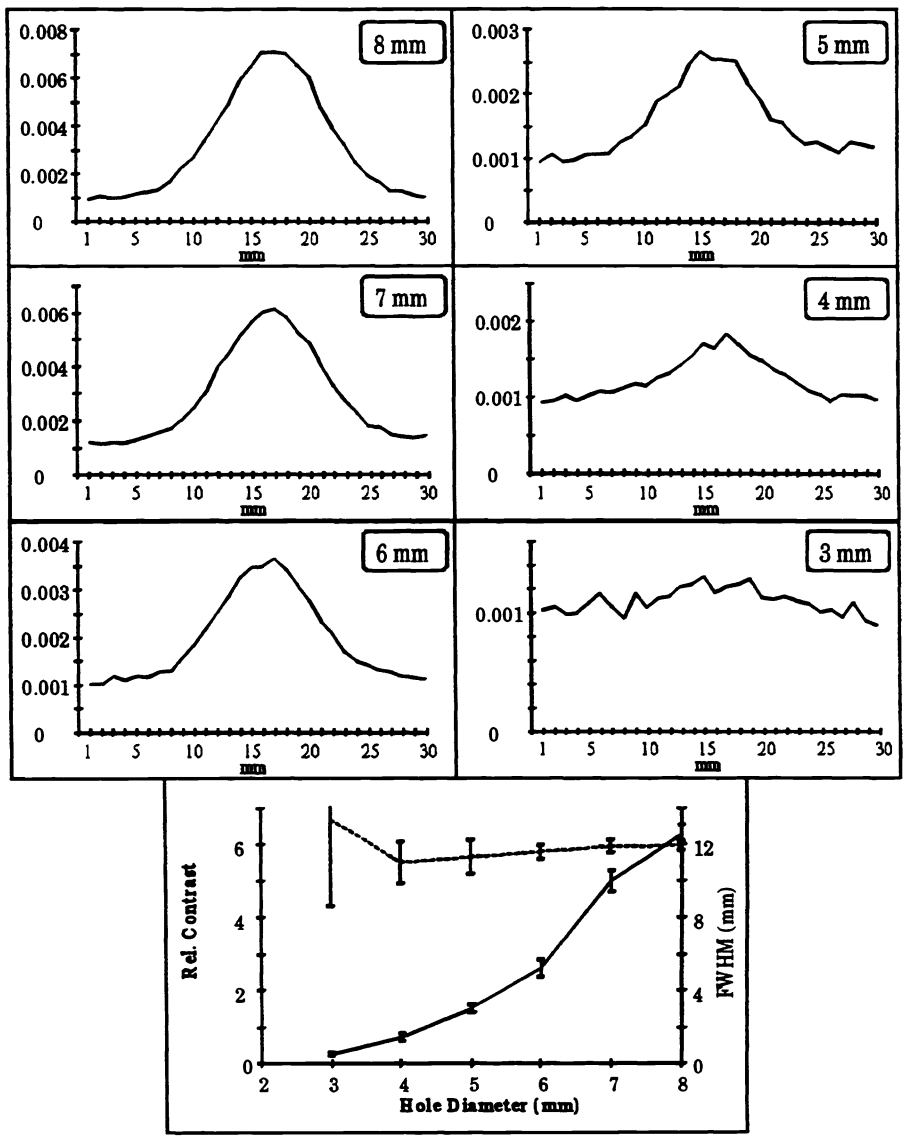

Fig. 4. Experimental curves obtained when transilluminating a 30 mm thick tissue phantom containing empty holes of different sizes, located in the middle. The lower diagram shows the relative contrast (solid line) and the FWHM (dashed line) as a function of the hole size.

3. Results

3.1 Gate width

In order to measure the effects of the time-gate width a 30 mm thick slab of Delrin with a 5 mm in diameter hole was used. The hole was located in the middle of the slab and was empty. We performed a scan over 30 mm transversally to the direction of the hole with 1 mm between every measuring point. The lower part of Fig. 2 shows the measurement geometry. The recording time was 10 sec per point. The upper part of Fig. 2 shows the light intensity in a 230 psec long gate divided by the total amount of light detected. This time gate corresponds to a light intensity of 0.1 % of the total light for regions far from the hole. This division is done to minimise the influence of some artefacts such as intensity variations in the laser and dirt on the sample surfaces. As can be seen there is more early light detected in the region with the hole than beside it. This effect has been shown in earlier studies and is due to the low scattering coefficient in the hole. In order to express the obtained scan in some figures, a fit to a Gaussian curve was performed. It turns out that the obtained scan fits a Gaussian curve very well. Some letters are introduced in the figure to express some features of the scan. A is the relative amount of light obtained off the empty hole. B is the increase of the relative amount of light in the empty hole region. C is the full

Downloaded from SPIE Digital Library on 01 Jul 2011 to 130.235.188.41. Terms of Use: http://spiedl.org/terms

width half maximum (FWHM) of the obtained scan. In Fig. 3 it is shown how these parameters change when the time-gate width is changed. Fig. 3a. shows the relative amount of light obtained at different gate widths (A). The time zero is chosen where the intensity starts to rise above the noise level. Fig. 3b. shows the relative contrast, i.e. B/A. As can be seen the shorter time-gate the higher contrast. Fig. 3c. shows the FWHM (C) of the scan while Fig. 3d. shows the residual from the least square fit of the Gaussian curve and the scan, i.e. this curve shows the "noise". As can be seen the noise is low down to about 200 psec. time-gate width, where the noise starts to rise. When we evaluated the experimental curves we chose a time-gate width where the relative amount of light is 0.1 percent far from the hole. This was equivalent with a width of approximately 230 psec., i.e. where the noise starts to rise.

3.2 Effects of hole size

In order to determine the spatial resolution of the system a series of scans with different hole sizes was performed. The geometry and size of the phantom was exactly as described in the previous paragraph. The diameter of the empty hole was altered between 8 and 3 mm. Fig. 4 shows typical scans obtained with the different hole sizes. As can be seen the hole can be seen down to a size of about 4 mm. The lower figure shows the relative contrast (B/A) and the FWHM (C) of the different scans. The curves are an average of five scans with error bars. As can be seen the contrast is very dependent of the size of the hole but the FWHM is not.

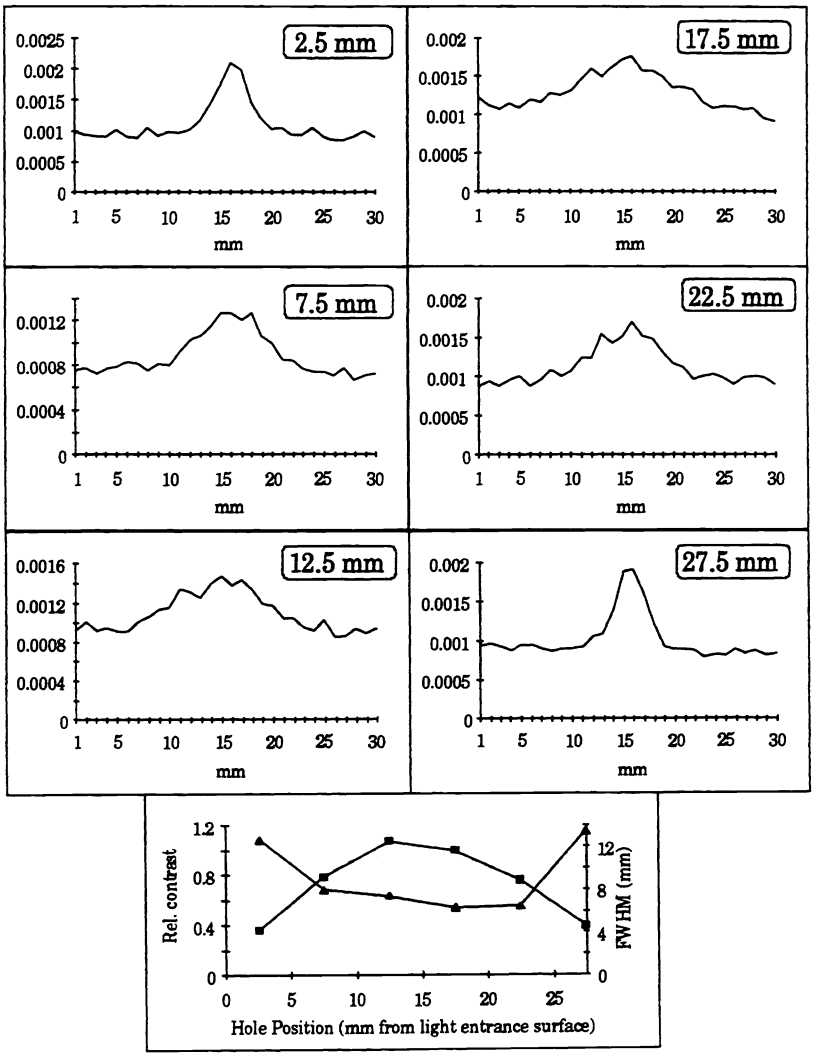

Fig. 5. Experimental curves obtained when transilluminating a 30 mm thick tissue phantom containing a 4 mm hole located at different distances from the surface where the light enters the phantom. The lower diagram shows the relative contrast (triangles) and the FWHM (squares) as a function of the hole position.

Downloaded from SPIE Digital Library on 01 Jul 2011 to 130.235.188.41. Terms of Use: http://spiedl.org/terms

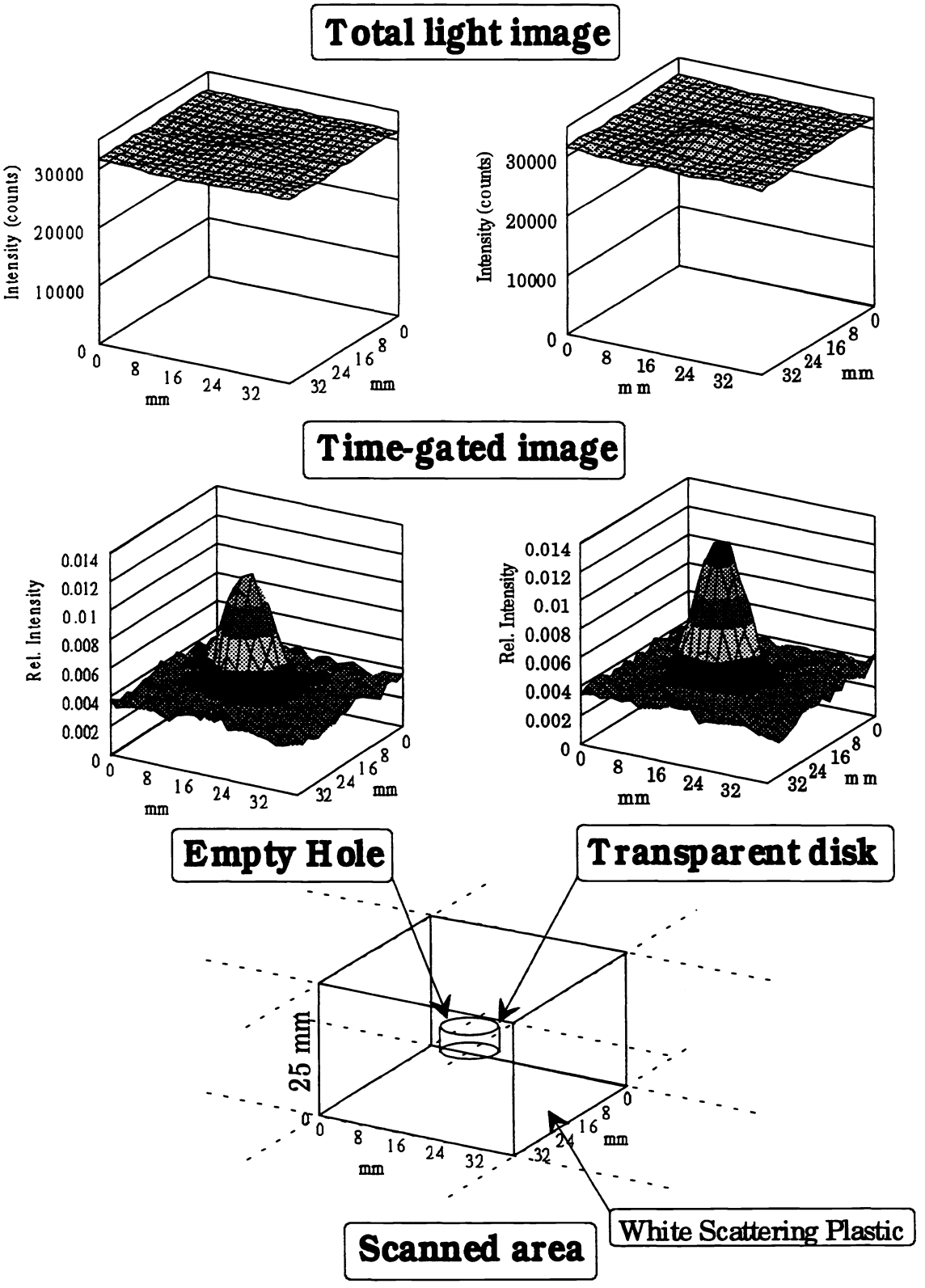

Fig. 6. 2-D scan over a 25 mm thick tissue phantom containing an empty hole (left) and a transparent disk of plexi glass.

Downloaded from SPIE Digital Library on 01 Jul 2011 to 130.235.188.41. Terms of Use: http://spiedl.org/terms

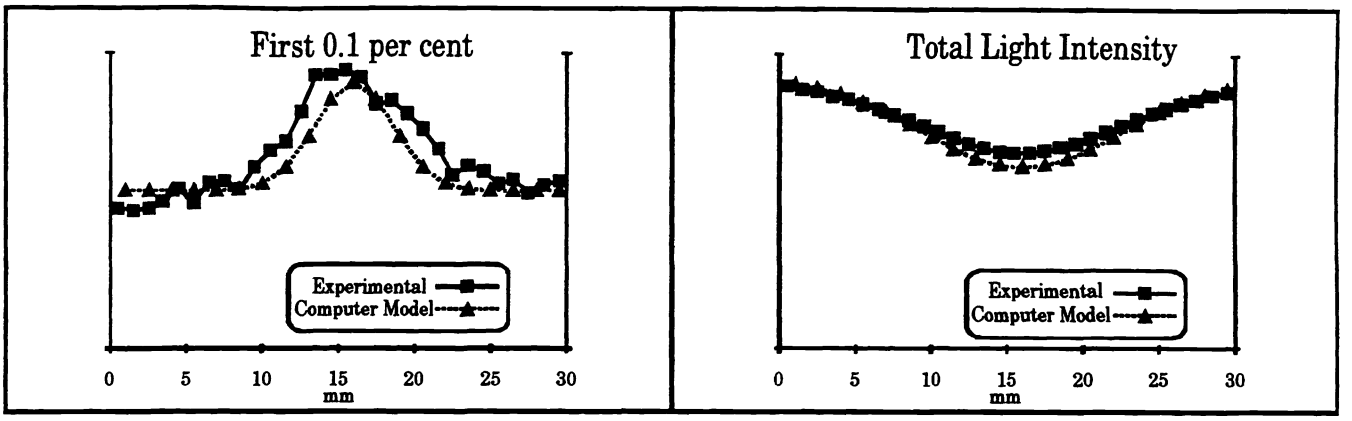

Fig. 7. Comparison between experimental results and the numerical computer model when transilluminating a 30 mm thick tissue phantom containing a 5 mm hole filled with a liquid that has lower scattering coefficient and higher absorption coefficient compared to the phantom.

3.3 Effects of hole position

We also wanted to study the influence of the position of the hole in the phantom. Fig. 5 shows the scans obtained when a 4 mm hole was located at different positions. The lower curves show the relative contrast and the FWHM as a function of the hole position. As can be seen the hole is most difficult to detect when it is located in the middle of the phantom.

3.4 Influence of refractive index

We wanted to verify that the observed increase of light on the hole is due to lack of scattering and not due to a change in the refractive index (since the hole was empty). A two-dimensional scan was achieved over a 25 mm thick phantom in which a 10 mm in diameter hole, 5 mm high, was located in the middle (See Fig. 6, lower part). A 40*40 mm large area was scanned with 2 mm between every point. The measuring time at each point was 2 seconds. The two left figures of Fig. 6 show the result when the hole was empty. The upper figure shows the total light intensity, i.e. the integral of each time dispersion curve. The lower figure shows the first 0.4 percent of each time dispersion curve divided by the total. The time-gate is a little longer in this experiment since the measuring time is shorter and thus the curves are noisier. As can be seen the empty hole can be clearly located in the time-gated image but it can hardly be noticed in the total light image. The two right figures of Fig. 6 show the same type of scan, but here the empty hole is filled with a piece of transparent plexi glass. The figures are very similar to the previous. This indicates that the increase of the early light on the hole is due to the lack of scattering and is not due to a higher speed of the light. It is also noticeable that the time-gated image obtained with the transparent disk shows a little higher intensity compared to the case with the empty hole. This is probably due to the fact that in the empty hole case some more scattering events take place due to the difference in refractive indices at the plastic-air boundaries.

3.5 Numerical modelling

The numerical computer model was compared to experimental results in order to verify the model. A scan was performed over a 30 mm thick slab of Delrin with a 5 mm diameter hole in the middle. The hole was filled with a mix between Intralipid and a laser dye (Rd 700). The optical properties of the two constituents were estimated by doing a simple narrow beam experiment on very diluted samples of each constituent. The optical properties of the mixture was estimated to μ_s'=0.56 mm^{-1} and μ_a=0.051 mm^{-1}, i.e. the cylinder had lower scattering and higher absorption than the surrounding Delrin. The numerical model was used to simulate the same type of scan. Fig. 7 shows the scans. The solid curves with boxes show the experimental result and the dashed curves with triangles show the result obtained with the numerical model. The left curve show the first 230 psec. of the light and the right figure show the total light intensity obtained at each measurement point. As can be seen the total light decreases when the scan passes over the cylinder due to the increased absorption, while the time-gated light intensity increases due to the lower scattering in the cylinder. For the numerical solutions calculated in this study a (x=31, y=31, z=20) matrix was used. To obtain a time dispersion curve with approximately 6 nsec. resolution, a computer time of 1 hour was required on a 33 MHz 486 processor PC.

Downloaded from SPIE Digital Library on 01 Jul 2011 to 130.235.188.41. Terms of Use: http://spiedl.org/terms

4. Discussion

Our experiments show that the influence of scattering is very high when performing time-gated viewing. Fig. 3 shows that an object with a scattering coefficient different from the surrounding could be detected using time-resolved detection techniques. This would not be possible in the steady-state case. Furthermore, in the geometry used here, an increased spatial resolution can be achieved due to the suppression of multiple scattered light. Our experiment show that it is possible to detect sub-cm features inside a for mammography realistically thick, highly scattering phantom. The phantom we used is a "worst case" for transillumination: the scattering is very high and the absorption is very low. Fig. 4 shows that the relative contrast of a hole in the centre of the phantom was very dependent on the hole size. A hole less than approximately 4 mm could not be detected. The full width of half maximum of the detected peak was rather constant for the different hole diameters. We believe that this reflects the highest spatial resolution detectable in this time window. We also show that the depth of the lesion is of great importance for detecting it. The closer to one of the borders the easier it is to detect. This is what you find in traditional diaphanography also.

5. Acknowledgements

This work was supported by the Swedish Research Council for Engineering Sciences, the Swedish Board for Industrial and Technical Developments and the Swedish Cancer Foundation (RMC).

6. References

1. *Medical Optical Tomography: Functional Imaging and Monitoring*, G. J. Müller, ed., SPIE Institute Series vol. 11 (Bellingham, WA, 1993).

2. R. J. Bartrum and H. C. Crow, "Transillumination lightscanning to diagnose breast cancer: A feasibility study," *Am. J. Rad.* **142**, 409-414 (1984).

3. M. Swift, D. Morrell, R. B. Massey and C. L. Chase, "Incidence of cancer in 161 families affected by ataxia-telangiectasia," *New Engl. J. Med.* **325**, 1831-1836 (1991).

4. B. C. Wilson, M. S. Patterson, S. T. Flock and D. R. Wyman, "Tissue Optical Properties in Relation to Light Propagation Models and in Vivo Dosimetry," in *Photon Migration in Tissue*, B. Chance, ed. (Plenum, New York, 1989) pp. 24-42.

5. S. Andersson-Engels, R. Berg, S. Svanberg and O. Jarlman, "Time-resolved transillumination for medical diagnostics," *Opt. Lett.* **15**, 1179-1181 (1990).

6. *Time-Resolved Spectroscopy and Imaging of Tissue*, B. Chance, ed., SPIE vol. 1431 (1991).

7. K. G. Spears, J. Serafin, N. H. Abramson, X. Zhu and H. Bjelkhagen, "Chrono-coherent imaging for medicine," IEEE Trans. *Biomed. Eng.* **36**, 1210-1221 (1989).

8. H. Chen, Y. Chen, D. Dilworth, E. Leith, J. Lopez and J. Valdmanis, "Two-dimensional imaging through diffusing media using 150-fs gated electronic holography techniques," *Opt. Lett.* **16**, 487-489 (1991).

9. K. M. Yoo, Q. Xing and R. R. Alfano, "Imaging objects hidden in highly scattering media using femtosecond second-harmonic-generation cross-correlation time gating," *Opt. Lett.* **16**, 1019-1021 (1991).

10. L. M. Wang, P. P. Ho, and R. R. Alfano, "Double-stage picosecond Kerr gate for ballistic time-gated optical imaging in turbid media," Appl. Opt. **32**, 535-540 (1993).

11. M. D. Duncan, R. Mahon, L. L. Tankersley and R. Reintjes, "Time-gated imaging through scattering media using stimulated Raman amplification," *Opt. Lett.* **16**, 1868-1870 (1991).

Downloaded from SPIE Digital Library on 01 Jul 2011 to 130.235.188.41. Terms of Use: http://spiedl.org/terms

12. J. C. Hebden, and K. S. Wong, "Time-resolved optical tomography," Appl. Opt. **32,** 372-380 (1993).

13. S. Andersson-Engels, R. Berg, A. Persson, and S. Svanberg, "Multispectral tissue characterization with time-resolved detection of diffusely scattered white light," *Opt. Lett.* **18,** (in press).

14. R. Berg, O, Jarlman, S. Svanberg, "Medical transillumination using short-pulse diode lasers," *Appl. Opt.* **32,** 574-579 (1993).

15. J. Fishkin, E. Gratton, M. J. vandeVen and W. W. Mantulin, "Diffusion of intensity modulated near-infrared light in turbid media," in *Time-Resolved Spectroscopy and Imaging of Tissue*, B. Chance, ed., SPIE vol. 1431, 122-135 (1991).

16. A. Knüttel, J. M. Schmitt, and J. R. Knutson, "Spatial localization of absorbing bodies by interfering diffusive photon-density waves," Appl. Opt. **32,** 381-389 (1993).

17. B. Chance, J. S. Leigh, H. Miyake, D. S. Smith, S. Nioka, R. Greenfeld, M. Finander, K. Kaufmann, W. Levy, M. Young, P. Cohen, H. Yoshioka and R. Boretsky, "Comparison of time-resolved and -unresolved measurements of deoxyhemoglobin in brain," *Proc. Natl. Acad. Sci. USA* **85**, 4971-4975 (1988).

18. D. T. Delpy, M. Cope, P. van der Zee, S. Arridge, S. Wray and J. Wyatt, "Estimation of optical pathlength through tissue from direct time of flight measurement," *Phys. Med. Biol.* **33**, 1433-1442 (1988).

19. R. Berg, S. Andersson-Engels, O. Jarlman and S. Svanberg, "Time-resolved transillumination for medical diagnostics," in *Time-Resolved Spectroscopy and Imaging of Tissue*, B. Chance, ed., SPIE vol. 1431, 110-119 (1991).

20. S. Andersson-Engels, R. Berg and S. Svanberg, "Effects of optical constants on time-gated transillumination of tissue and tissue-like media," *J. Photochem. Photobiol.* **16**, 155-167 (1992).

21. M. S. Patterson, B. Chance and B. C. Wilson, "Time resolved reflectance and transmittance for the non-invasive measurement of optical properties," *Appl. Opt.* **28**, 2331-2336 (1989).

22. S. L. Jacques, "Time resolved propagation of ultrashort laser pulses within turbid tissue," Appl. Opt. **28.** 2223-2229 (1989).

23. M. S. Patterson, S. J. Madsen, J. D. Moulton, B. C. Wilson, "Diffusion equation representation of photon migration in tissue," *IEEE MTT-S Digest,* 905-908 (1991).

24. M. S. Patterson, J. D. Moulton, B. C. Wilson, K. W. Berndt and J. R. Lakowicz, "Frequency-domain reflectance for the determination of the scattering and absorption properties of tissue," *Appl. Opt.* **30**, 4474-4476 (1991).

Downloaded from SPIE Digital Library on 01 Jul 2011 to 130.235.188.41. Terms of Use: http://spiedl.org/terms